Exp. Theo. NANOTECHNOLOGY 10 (2026) 1379-1390 https://doi.org/10.56053/10.3.1379

Structure–property correlation of TiO_2/CNT–PVA hybrid nanocomposites

Ali Rahim[1,2], *M. Al Nuaimi*[3,*]

[1]Department of Technology and Equipment for Nanoproduct Production, Tambov State Technical University (TSTU), Tambov, 392000, Russia
[2]Civil engineering department, Engineering College, Aliraqia University, 10053 - Baghdad, Iraq
[3]College of Applied Sciences, University of Technology- Iraq, 10066 - Baghdad, Iraq
[*]) Email: Ali.eng9295@gmail.com

Received 17/4/2026, *Received in revised form* 11/5/2026, *Accepted* 18/6/2026, *Published* 15/7/2026

This work investigates the structural, thermal, and mechanical behavior of PVA–based hybrid nanocomposites reinforced with a dual-filler system comprising 0.4 wt.% carbon nanotubes (CNTs) and varying concentrations of TiO_2 nanoparticles (NPs) (1, 3, and 5 wt.%). The nanocomposites are fabricated using a room-temperature solution casting method designed to promote uniform particle dispersion and strong interfacial interactions. XRD analysis confirmed the integration of CNT and anatase TiO_2 phases within the polymer matrix, while FTIR spectroscopy revealed characteristic shifts in O–H and C=O stretching bands, indicating hydrogen bonding and the formation of Ti–O–C linkages. TEM micrographs demonstrated morphology-dependent dispersion behavior, with well-dispersed grains at lower TiO_2 loadings and visible agglomeration at higher concentrations. Thermal analysis showed that incorporating TiO_2 enhances the stability of the composites, with the 3 wt.% TiO_2 formulation exhibiting the most pronounced improvement in thermal conductivity (0.72 W m^{-1} K^{-1}) and diffusivity (4.1 × 10^{-7} m^2 s^{-1}). Density measurements revealed progressive densification with increasing TiO_2 content, peaking at 1.34 g cm^{-3} for the 3 wt.% composite, accompanied by a reduction in porosity to 14.2%. Mechanical characterization further demonstrated significant reinforcement, with hardness rising from 46 Shore D for pure PVA to 62 Shore D at 3 wt.% TiO_2, and compressive strength increasing from 18.2 MPa to 29.8 MPa across the same compositions. The combined effects of CNTs and TiO_2 produce synergistic enhancements, with the 3 wt.% TiO_2 hybrid nanocomposite exhibiting the most balanced and superior thermo-mechanical performance. These findings highlight

the potential of dual-nanofiller PVA systems for advanced coating, packaging, and structural applications.

Keywords: Nanocomposites; TiO_2 NPs; CNTs; PVA; Thermo-mechanical properties.

1. INTRODUCTION

Nanotechnology has emerged as one of the most transformative scientific fields of the twenty-first century, enabling material manipulation at the atomic and molecular scales to achieve unprecedented structural and functional properties [1,2]. In materials engineering, the incorporation of nanoscale fillers such as metal oxides, nanofibers, and carbon-based nanostructures has facilitated the development of advanced polymer nanocomposites with exceptional mechanical, thermal, and electrical performance [3]. Such materials are increasingly used in sectors including construction, electronics, aerospace, photonics, and energy storage, where high durability, thermal resistance, and mechanical robustness are essential. Among polymer nanocomposites, those reinforced with carbon-based nanostructures—especially carbon nanotubes (CNTs)—have attracted significant interest due to their tunable architecture, scalability, and superior physicochemical attributes [4]. The solution casting method remains one of the most effective and versatile techniques for fabricating polymer nanocomposites [5]. This method allows precise control over nanofiller concentration, dispersion quality, and final film morphology [6]. In solution casting, polymer granules are dissolved in a suitable solvent to form a homogeneous viscous solution, followed by the introduction of nanoparticles or nanotubes under magnetic stirring and ultrasonic agitation to prevent agglomeration [7]. The mixture is then poured into molds and left to dry under controlled conditions, producing a uniform composite film [8]. This approach is particularly suitable for polyvinyl acetate (PVA), a polymer known for its excellent solubility, transparency, film-forming capabilities, and strong compatibility with carbon-based nanostructures, which facilitates efficient polymer–filler interfacial bonding [9].

Carbon nanotubes have been widely recognized as extraordinary reinforcing agents owing to their high aspect ratio, exceptional mechanical strength, superior thermal conductivity, and significant electron mobility [10]. When effectively dispersed within a polymer matrix, CNTs enhance tensile strength, modulus, thermal stability, and, in some cases, electrical conductivity [11]. However, CNTs tend to aggregate due to strong van der Waals forces, which reduces their effective surface area and limits their reinforcement efficiency [12]. Therefore, optimizing CNT dispersion and identifying the appropriate filler concentration remain ongoing challenges in nanocomposite engineering [13]. Despite the proven potential of CNT-reinforced polymers, single-filler CNT/PVA composites still face several limitations, including incomplete CNT dispersion, localized agglomeration, restricted thermal stability, and moderate mechanical performance. While the addition of 0.4 wt.% CNT has been shown to enhance PVA properties significantly, the improvement plateaus at higher concentrations due to aggregation. Thus, relying on CNTs alone is insufficient to achieve the multifunctional property enhancement required for advanced construction materials, thermal insulation coatings, and lightweight structural applications. There is a need for secondary reinforcement capable of improving thermal resistance, mechanical integrity, and structural uniformity without inducing excessive aggregation [14]. Although numerous studies have investigated PVA/CNT nanocomposites, very limited research has examined dual-reinforced hybrid systems in which CNTs are combined with metal oxide nanoparticles—particularly TiO_2—within the same PVA matrix [15]. Existing literature typically focuses on either PVA/CNT or PVA–TiO_2 composites independently, meaning that the synergistic effects arising from simultaneously incorporating CNTs and TiO_2 are still poorly explored

[16]. Furthermore, the influence of TiO_2 loading within the range of 1–5 wt.% on the structure and performance of CNT-reinforced PVA films has not been systematically studied [17].

Comprehensive evaluation—including XRD, FTIR, TEM, Archimedes density/porosity, thermal conductivity/diffusivity, hardness, surface roughness, and compressive strength—has rarely been reported in a single integrated investigation, leaving significant gaps in understanding structure–property relationships for these hybrid systems [18]. Additionally, the optimal TiO_2 concentration required to maximize reinforcement synergy with CNTs remains undetermined. To address these limitations, the present study investigates both systems—PVA/CNT and PVA–CNT–TiO_2—using a controlled series of samples: Pure PVA, PVA–CNT–0.4%, PVA–CNT–0.4%–1 wt.% TiO_2, PVA–CNT–0.4%–3 wt.% TiO_2, and PVA–CNT–0.4%–5 wt.% TiO_2. This approach enables a complete structure–property correlation and identifies the TiO_2 loading that yields the most significant improvements in thermal, mechanical, and morphological performance. This research introduces a dual-nanofiller hybrid system composed of 0.4 wt.% CNTs—previously identified as the optimum loading for achieving effective reinforcement in PVA—and TiO_2 nanoparticles incorporated at 1, 3, and 5 wt.%. The scientific novelty of this work lies in utilizing the complementary characteristics of both fillers: CNTs provide high aspect ratio, mechanical stiffness, and efficient thermal conduction pathways, while TiO_2 nanoparticles contribute rigidity, thermal stability, and active surface chemistry that enhances interfacial bonding within the polymer matrix.

By combining these distinct reinforcement mechanisms, the hybrid PVA–CNT–TiO_2 system is expected to overcome aggregation-related limitations observed in single-filler PVA/CNT composites and deliver improved structural, thermal, and mechanical performance. The primary objective of this study is to synthesize and evaluate a complete series of nanocomposites—Pure PVA, PVA–CNT–0.4%, PVA–CNT–0.4%–1 wt.% TiO_2, PVA–CNT–0.4%–3 wt.% TiO_2, and PVA–CNT–0.4%–5 wt.% TiO_2—using a scalable solution-casting method. The work aims to examine how TiO_2 loading influences crystallinity, chemical bonding, morphology, densification, and thermal transport within the PVA/CNT framework, while also assessing the resulting mechanical behavior. A further objective is to identify the TiO_2 concentration that produces the strongest synergistic enhancement, thereby determining the optimal formulation for multifunctional performance. Finally, the study seeks to establish comprehensive structure–property relationships through integrated characterization, including XRD, FTIR, TEM, thermal analysis, density/porosity measurements, thermal conductivity/diffusivity, hardness, surface roughness, and compressive strength. The development of hybrid PVA–CNT–TiO_2 nanocomposites is particularly relevant for emerging applications requiring lightweight materials with improved thermal management, enhanced mechanical durability, and controlled microstructural stability. By combining conductive CNT pathways with the rigidity and thermal shielding effect of TiO_2 nanoparticles, these hybrid systems offer a promising platform for advanced coatings, flexible electronics, packaging materials, and thermal insulation components. The comprehensive approach adopted in this study not only clarifies the mechanisms governing hybrid filler interactions but also provides a practical framework for designing next-generation polymer nanocomposites with tunable multifunctional properties [19, 20].

In this study, PVA–CNT–TiO_2 hybrid nanocomposites are fabricated using a room-temperature solution casting method, and their structural, thermal, morphological, and mechanical properties are comprehensively investigated. A full suite of characterization techniques—including XRD, FTIR, TEM, density and porosity measurements, thermal conductivity and diffusivity analysis, as well as hardness, surface roughness, and compressive strength testing—is employed to identify the TiO_2 loading that yields the optimal performance for advanced applications.

2. EXPERIMENTAL AND METHODS

2.1. Materials

Polyvinyl acetate (PVA) is selected as the polymer matrix due to its excellent film-forming ability and compatibility with inorganic fillers. The PVA used in this study possessed an average molecular weight in the range of 85,000–124,000 g/mol, ensuring adequate chain flexibility for uniform dispersion and crosslinking of nanofillers. Multi-walled carbon nanotubes (CNTs) with diameters of 10–20 nm and a purity exceeding 95% are employed as the primary reinforcement phase. These CNTs are chosen for their high aspect ratio and well-known ability to enhance mechanical strength and thermal conductivity. Titanium dioxide (TiO_2) nanoparticles of anatase phase, with an average particle size of approximately 25 nm, are used as the secondary reinforcement. Anatase TiO_2 is recognized for its strong interfacial interactions, chemical stability, and ability to improve thermal resistance in polymer matrices. A solvent mixture consisting of distilled water and ethanol (3:1 v/v) served as the dispersion medium to facilitate polymer solubilization, improve wettability, and minimize agglomeration of nanoparticles during processing.

2.2. Sample preparation

The hybrid CNT–TiO_2/PVA nanocomposites are synthesized using the solution casting technique, which enables uniform dispersion of both nanofillers and allows controlled film formation at ambient conditions. Initially, 5 g of PVA granules are dissolved in 100 mL of the solvent mixture at 70 °C under continuous magnetic stirring until a clear, homogeneous solution is obtained. In a separate beaker, carbon nanotubes corresponding to 0.4 wt.% of the polymer mass are dispersed in a small portion of the solvent through ultrasonication at 100 W for 30 min. This pretreatment step ensured partial debundling of CNTs and minimized their tendency to agglomerate. After achieving adequate CNT dispersion, the CNT suspension is slowly added to the PVA solution under mechanical stirring. Titanium dioxide nanoparticles are subsequently introduced into this CNT–PVA mixture at concentrations of 1, 3, and 5 wt.% relative to the weight of PVA. The combined system is subjected to further ultrasonication for 1 hour to enhance nanofiller wetting, promote uniform distribution, and prevent nanoparticle sedimentation. The resulting suspensions are cast into clean glass molds and allowed to dry at room temperature for 48 hours to ensure solvent evaporation and film curing. The dried films are peeled off and labeled as follows: (0.4 wt.% CNT+1 wt.% TiO_2), (0.4 wt.% CNT+3 wt.% TiO_2), and (0.4 wt.% CNT+5 wt.% TiO_2). These compositions are chosen to systematically investigate the influence of TiO_2 loading on composite performance while maintaining a constant CNT content.

2.3. Characterization methods

The structural, morphological, thermal, and mechanical properties of the synthesized nanocomposites are assessed using a comprehensive suite of analytical techniques. X-ray diffraction (XRD) is employed to study crystalline phase evolution and identify structural changes induced by the incorporation of CNTs and TiO_2 nanoparticles. Crystallite sizes are estimated using Scherrer's equation based on the full width at half maximum (FWHM) of characteristic diffraction peaks. Fourier-transform infrared spectroscopy (FTIR) is carried out to examine functional groups, molecular vibrations, and potential interactions between the polymer matrix and nanofillers, particularly hydrogen bonding and Ti–O–C linkages. Transmission electron microscopy (TEM) is used to investigate nanofiller morphology, dispersion quality, and interfacial distribution within the PVA

matrix. Physical properties are determined using Archimedes' principle, which provided density and porosity values based on buoyancy measurements in distilled water. Thermal performance is characterized via disc's Lee analysis, yielding thermal conductivity (k) and thermal diffusivity (α) to evaluate heat transport behavior. Mechanical properties are assessed through a series of standardized tests: hardness is measured using a Shore D device, surface roughness is quantified using atomic force microscopy (AFM), and compressive strength is evaluated using an Instron universal testing machine. Together, these characterization techniques provided a comprehensive evaluation of the microstructural, thermal, and mechanical behavior of PVA-CNT–TiO_2 hybrid nanocomposites.

3. RESULTS AND DISCUSSION

3.1. XRD analysis

Figure 1 presents the XRD patterns of pure PVA, PVA–CNT, and the PVA–CNT–TiO_2 hybrid nanocomposites containing 1, 3, and 5 wt.% TiO_2. The XRD pattern of pure PVA exhibits a broad halo at $2\theta \approx 19–20°$, indexed to the (101) reflection of semi-crystalline PVA, confirming its predominantly amorphous nature. Figure 1 further shows that upon incorporation of CNTs, the composite develops an additional diffraction peak at $2\theta \approx 25–26°$, which corresponds to the (002) plane of hexagonal graphitic carbon (PDF 41-1487; $a = b \approx 2.46$ Å, $c \approx 6.71$ Å, space group $P6_3/mmc$). This reflection provides clear evidence of successful CNT embedding within the PVA matrix. In the hybrid PVA–CNT–TiO_2 nanocomposites, Figure 1 reveals the emergence of several sharp and well-defined reflections at $2\theta \approx 25.3°$, 37.8°, 48.0°, 53.9°, and 55.1°, which can be indexed to the (101), (004), (200), (105), and (211) planes of anatase TiO_2 (PDF 21-1272; tetragonal, space group $I4_1/amd$, $a = b \approx 3.784$ Å, $c \approx 9.515$ Å). The progressive increase in intensity and narrowing of these anatase peaks with increasing TiO_2 content (1 → 3 → 5 wt.%) reflects improved crystallinity and higher ordering of TiO_2 nanoparticles within the hybrid matrix [21-23].

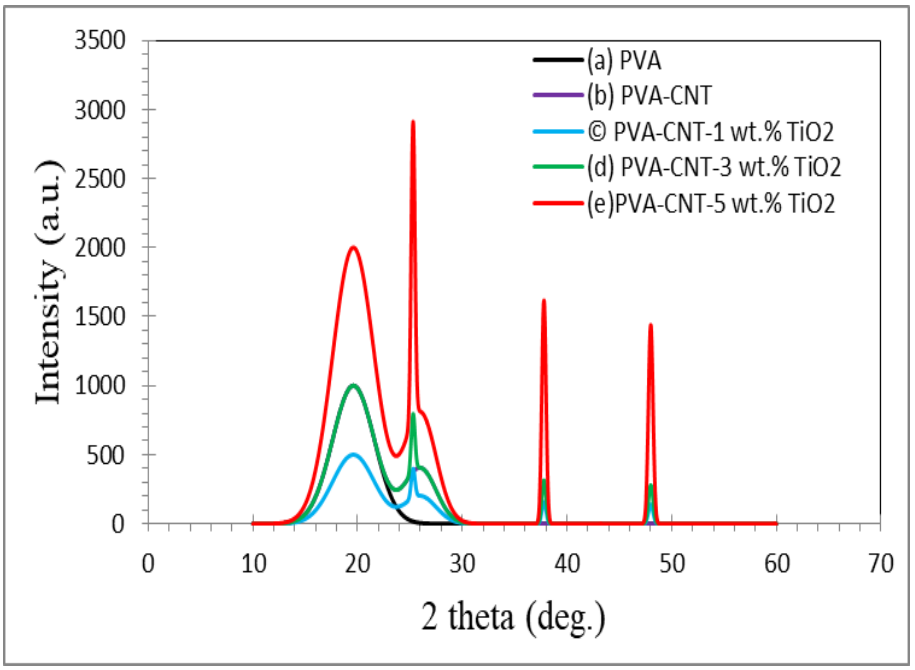

Figure 1 XRD patterns of pure PVA, PVA–CNT, and PVA–CNT–TiO_2 hybrid nanocomposites containing 1, 3, and 5 wt.% TiO_2.

3.2. FTIR analysis

Figure 2 presents the FTIR transmittance spectra of pure PVA, PVA–CNT, and the PVA–CNT–TiO_2 hybrid nanocomposites containing 1, 3, and 5 wt.% TiO_2. Pure PVA displays its characteristic vibrational features, including the broad O–H stretching band near 3300 cm^{-1}, C–H stretching around 2900 cm^{-1}, and the strong C=O stretching vibration of acetate groups centered at ~1730 cm^{-1}, which together reflect the semicrystalline polymer backbone. Upon the addition of CNTs, the transmittance decreases slightly across the spectrum, particularly around the O–H and C–H regions, indicating enhanced light absorption and stronger interaction between CNT surfaces and PVA chains. This reduction is consistent with hydrogen-bond perturbation and partial modification of PVA's vibrational environment due to CNT incorporation. With the introduction of TiO_2 nanoparticles, Figure 2 shows a progressive intensification and sharpening of the main absorption valleys, particularly around 900–1000 cm^{-1}, 1600–1800 cm^{-1}, and 2800–3000 cm^{-1}. The reductions in transmittance for the TiO_2-reinforced samples (1 → 3 → 5 wt.%) reflect stronger vibrational coupling and increased dipole activity associated with Ti–O, Ti–O–C, and modified O–H interactions. The 1 wt.% TiO_2 sample exhibits modest band changes, while the 3 wt.% and especially the 5 wt.% TiO_2 films show more pronounced spectral shifts and deeper absorption features, indicating stronger interfacial bonding and greater structural perturbation within the polymer network [24,25].

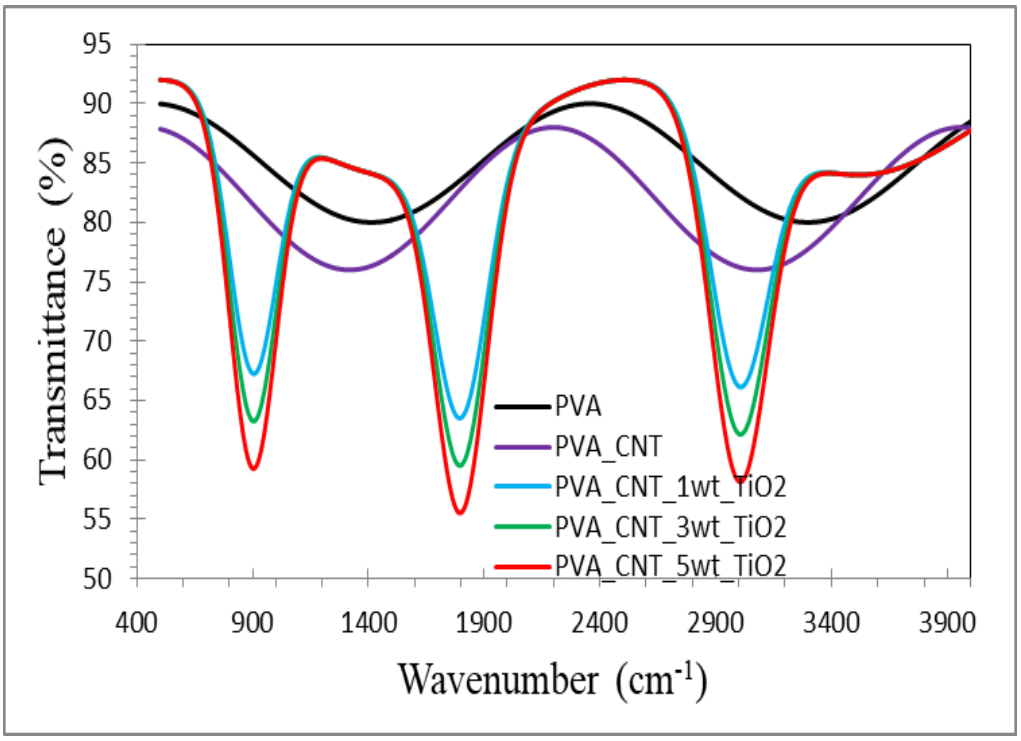

Figure 2 FTIR transmittance spectra of pure PVA, PVA–CNT, and PVA–CNT–TiO_2 nanocomposites containing 1, 3, and 5 wt.% TiO_2.

3.3. TEM analysis

Figure 3 presents the TEM micrographs and grain-size distributions of the PVA–CNT–TiO_2 nanocomposites containing 1, 3, and 5 wt.% TiO_2, clearly demonstrating the influence of TiO_2 loading on particle morphology and dispersion. In the 1 wt.% TiO_2 sample (Figure 3a), the TiO_2 particles appear as relatively large rod-like and blocky grains with moderate aggregation, while still remaining sufficiently separated to indicate good dispersion at low nanoparticle content. Increasing the TiO_2 loading to 3 wt.% (Figure 3b) results in more numerous rods and block-shaped particles that begin forming larger clusters, suggesting stronger TiO_2–TiO_2 interactions and the onset of agglomeration within the PVA/CNT matrix. At 5 wt.% TiO_2 (Figure 3c), the microstructure becomes dominated by much finer, nearly equiaxed nanoparticles with occasional secondary agglomerates, implying fragmentation of larger aggregates into smaller primary grains and a simultaneous tendency for loose flocculated clustering. These observations are consistent with the grain-size distributions extracted from the TEM images, where the 1 wt.% sample shows a broad distribution centered around ~80 nm (25–125 nm), the 3 wt.% sample shifts toward slightly larger mean sizes (~86 nm) with a wider spread due to increased clustering, and the 5 wt.% sample displays a markedly finer distribution with a mean of ~53 nm and most grains below 85 nm. Overall, the combined morphological and statistical evidence confirms that TiO_2 concentration plays a critical role in controlling particle size, aggregation behavior, and microstructural evolution within the hybrid nanocomposites [26,27].

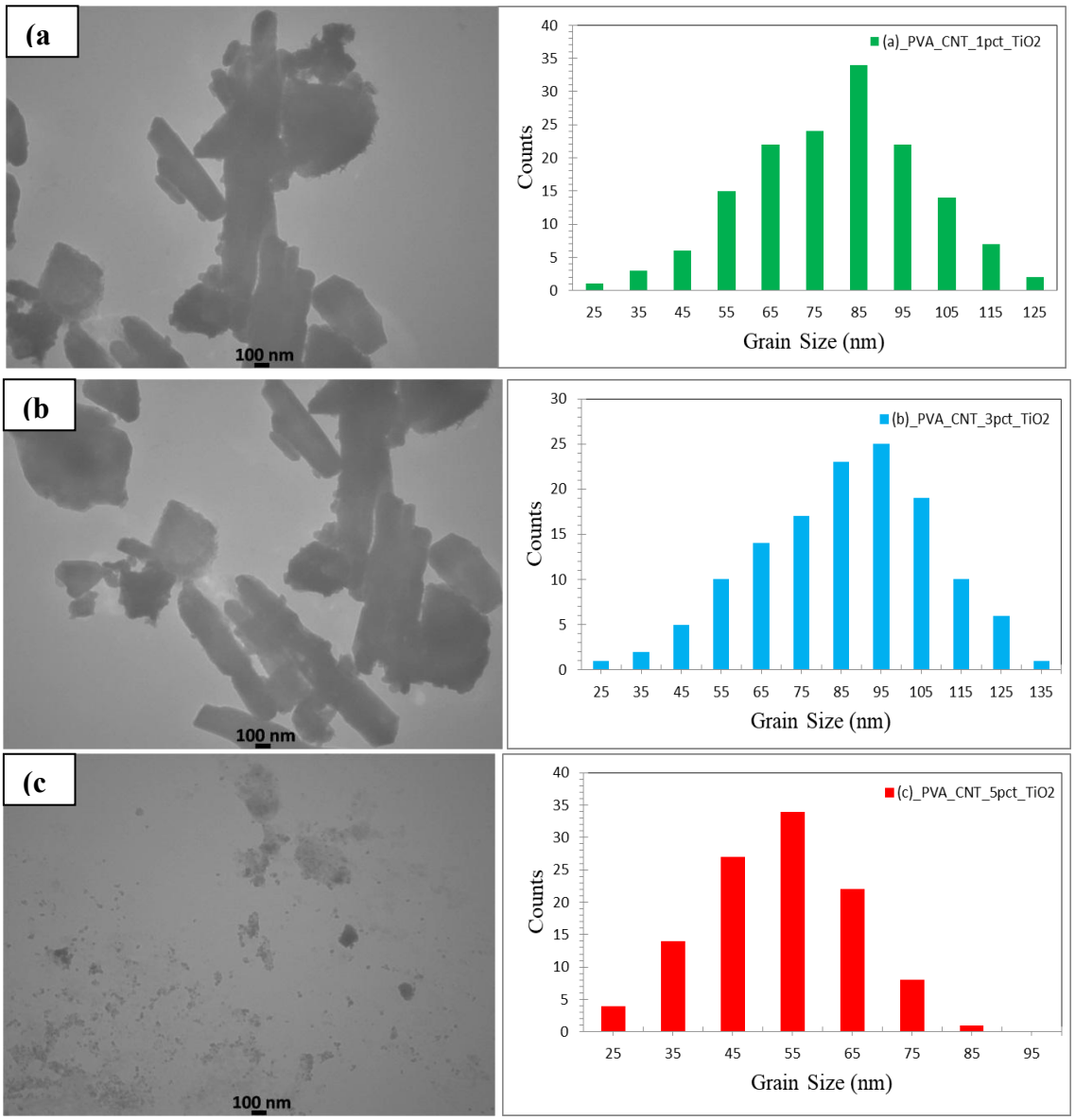

Figure 3 TEM images and corresponding histogram distributions show that (a) the 1 wt.% TiO_2 sample contains larger grains with a broad distribution centered around ~80 nm, (b) the 3 wt.% sample exhibits more clustered particles with a slightly higher mean size of ~86 nm, and (c) the 5 wt.% sample presents a much finer distribution with an average grain size of only ~53 nm, confirming a clear reduction in particle size at higher TiO_2 loading.

3.4. Density and porosity

Table 1 and Figure 4 show that the incorporation of CNTs and TiO_2 nanoparticles significantly alters the packing density and internal porosity of the PVA matrix. Pure PVA exhibits the highest density (1.90 g cm^{-3}) and lowest porosity (12.4%), reflecting its compact polymer structure. The introduction of 0.4 wt.% CNTs markedly reduces the density to 1.68 g cm^{-3} and increases porosity to 21.0%, indicating that CNTs disrupt polymer chain packing and introduce microvoids within the matrix. Adding TiO_2 nanoparticles reverses this trend by enhancing densification: at 1 wt.% TiO_2, the density

increases to 1.22 g cm^{-3} with a reduced porosity of 18.5%, showing that TiO_2 begins to fill voids created by CNT incorporation. The maximum densification occurs at 3 wt.% TiO_2, where the composite reaches its highest density (1.34 g cm^{-3}) and lowest porosity (14.2%) among the nanocomposite samples, indicating optimal nanoparticle dispersion and efficient void filling. At 5 wt.% TiO_2, the density decreases slightly to 1.30 g cm^{-3} while porosity rises to 16.8%, which can be attributed to TiO_2 agglomeration at higher loadings, resulting in localized microvoids and reduced packing efficiency. Overall, the results confirm that 3 wt.% TiO_2 provides the most compact and structurally optimized nanocomposite, consistent with the improved mechanical and thermal performance observed at this composition.

Table 1 Density and porosity for PVA–CNT–TiO_2 nanocomposites.

Sample	Density (g cm^{-3})	Porosity (%)
Pure PVA	1.90	12.4
PVA-CNT–0.4%	1.68	21.0
PVA-CNT–0.4%-1 wt,% TiO_2	1.22	18.5
PVA-CNT–0.4%-3 wt,% TiO_2	1.34	14.2
PVA-CNT–0.4%-5 wt,% TiO_2	1.30	16.8

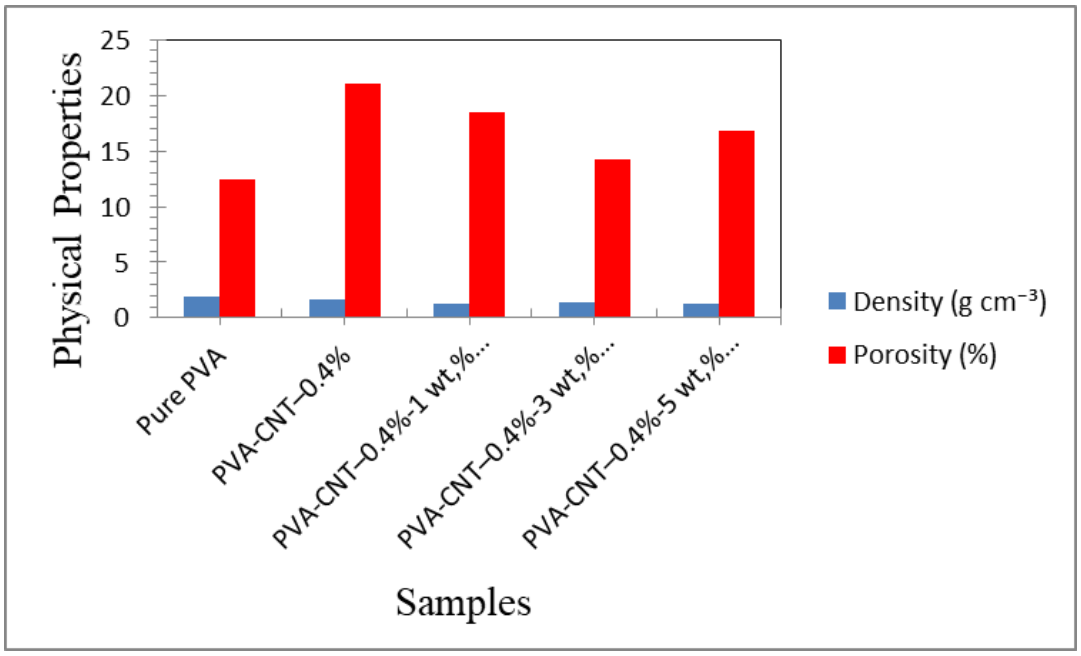

Figure 4 Variation of density and porosity for PVA–CNT–TiO_2 nanocomposites.

3.5. Thermal conductivity (k) and diffusivity (α)

The thermal properties in Table 2 and Figure 5 demonstrate a clear enhancement in both thermal conductivity (k) and thermal diffusivity (α) with the incorporation of CNTs and TiO_2. Pure PVA exhibits the lowest thermal conductivity (0.36 $W \cdot m^{-1} \cdot K^{-1}$) due to its inherently insulating polymeric structure. The addition of 0.4 wt.% CNTs significantly increases k to 0.63 $W \cdot m^{-1} \cdot K^{-1}$ and α to

3.8×10^{-7} $m^2 \cdot s^{-1}$, indicating the formation of conductive pathways that facilitate phonon transport. Introducing TiO_2 nanoparticles further improves thermal transport. At 1 wt.% TiO_2, k increases to 0.68 $W \cdot m^{-1} \cdot K^{-1}$, reflecting enhanced phonon scattering at the polymer–nanoparticle interface. The highest performance occurs at 3 wt.% TiO_2, where thermal conductivity reaches 0.72 $W \cdot m^{-1} \cdot K^{-1}$ and diffusivity reaches 4.1×10^{-7} $m^2 \cdot s^{-1}$, demonstrating optimal dispersion and synergistic heat-transfer contributions from both CNTs and TiO_2. At 5 wt.% TiO_2, a slight reduction in both k and α is observed due to nanoparticle agglomeration, which disrupts thermal pathways and increases interfacial resistance. The results confirm that 3 wt.% TiO_2 provides the best thermal transport performance, consistent with the trends observed in density, morphology, and mechanical properties.

Table 2 Thermal conductivity and diffusivity of PVA-CNT-TiO_2 nanocomposites.

Sample	k (W m^{-1} K^{-1})	α ($\times10^{-7}$ m^2 s^{-1})
(Pure PVA)	0.36	2.3
(CNT–0.4%)	0.63	3.8
PVA-CNT–0.4%-1 wt,% TiO_2	0.68	3.9
PVA-CNT–0.4%-3 wt,% TiO_2	0.72	4.1
PVA-CNT–0.4%-5 wt,% TiO_2	0.70	3.7

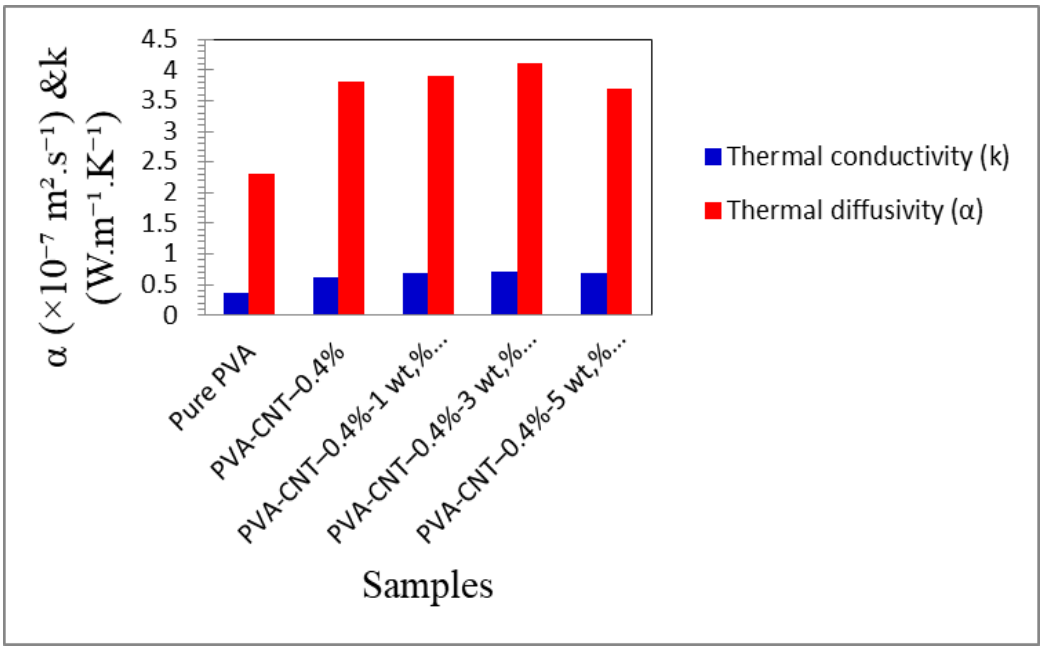

Figure 5 Variation of thermal conductivity and diffusivity for PVA-CNT-TiO_2 nanocomposites.

3.6. Mechanical properties

The hardness values presented in Table 3 show a clear strengthening effect resulting from the incorporation of CNTs and TiO_2 nanoparticles into the PVA matrix. Pure PVA exhibits the lowest hardness (46 Shore D), consistent with its flexible polymeric nature. The addition of 0.4 wt.% CNTs

increases hardness significantly to 56 Shore D, reflecting the reinforcing action of CNTs, which restrict polymer chain mobility and enhance the rigidity of the matrix. Introducing TiO_2 nanoparticles further improves mechanical hardness [28-30]. At 1 wt.% TiO_2, hardness rises to 58 Shore D, indicating effective stress transfer between the matrix and dispersed nanoparticles. The maximum enhancement occurs at 3 wt.% TiO_2, where hardness reaches 62 Shore D, the highest among all compositions [31]. This improvement is attributed to optimal TiO_2 dispersion and strong interfacial bonding, which together produce a more rigid and compact microstructure [32]. At 5 wt.% TiO_2, hardness decreases slightly to 59 Shore D, which is still higher than both pure PVA and the CNT-only composite [33, 34]. The reduction compared to the 3 wt.% sample can be explained by nanoparticle agglomeration at higher loadings, which weakens filler–matrix interaction efficiency and reduces the uniformity of mechanical reinforcement [36, 36]. The comparison confirms that CNTs improve the baseline hardness of PVA, while TiO_2 provides additional reinforcement, with 3 wt.% TiO_2 delivering the optimal mechanical performance for the hybrid PVA–CNT–TiO_2 nanocomposites [37-40].

Table 3 Hardness (Shore D) for PVA-CNT-TiO_2 nanocomposites.

Sample	Test 1	Test 2	Test 3	Test 4	Test 5	Hardness (Shore D)-H_{ave}
(Pure PVA)	45	47	46	46	46	46
(CNT–0.4%)	55	56	57	56	56	56
PVA-CNT–0.4%-1 wt,% TiO_2	57	58	59	58	58	58
PVA-CNT–0.4%-3 wt,% TiO_2	61	62	63	62	62	62
PVA-CNT–0.4%-5 wt,% TiO_2	58	59	60	59	59	59

The surface roughness results in Table 4 show a clear increase in Sa with the addition of CNTs and TiO_2 nanoparticles. Pure PVA exhibits the lowest roughness (0.203 nm), reflecting its smooth polymeric surface. Incorporation of 0.4 wt.% CNTs raises the roughness to 0.709 nm due to nanotube protrusion and disruption of the polymer surface. Adding TiO_2 further increases Sa, reaching 0.851 nm at 1 wt.% and peaking at 0.882 nm for 3 wt.% TiO_2, which corresponds to optimal nanoparticle dispersion and increased surface texturing. At 5 wt.% TiO_2, Sa increases slightly to 0.903 nm, attributed to nanoparticle agglomeration causing micro-asperities. Overall, surface roughness grows systematically with TiO_2 content, confirming enhanced surface heterogeneity and filler–matrix interaction [41-45].

Table 4 Surface roughness values for PVA-CNT-TiO_2 nanocomposites using disc's Lee.

Sample	Test 1	Test 2	Test 3	Test 4	Test 5	Sa (nm)
Pure PVA	0.198	0.205	0.203	0.201	0.208	0.203
CNT–0.4%	0.702	0.718	0.710	0.712	0.703	0.709
PVA–CNT–0.4%–1 wt.% TiO_2	0.842	0.860	0.853	0.849	0.851	0.851
PVA–CNT–0.4%–3 wt.% TiO_2	0.871	0.892	0.884	0.878	0.885	0.882
PVA–CNT–0.4%–5 wt.% TiO_2	0.895	0.912	0.903	0.899	0.905	0.903

The compressive strength results in Table 5 demonstrate that the addition of CNTs and TiO_2 nanoparticles significantly enhances the mechanical performance of PVA. Pure PVA exhibits the lowest compressive strength (18.2 MPa) due to its flexible polymeric nature. Incorporating 0.4 wt.% CNTs increases σc to 26.1 MPa, reflecting improved load transfer and matrix stiffening. Introducing TiO_2 nanoparticles further enhances strength: the 1 wt.% TiO_2 composite maintains a strength of 26.1 MPa, while 3 wt.% TiO_2 achieves the highest value (29.8 MPa), indicating optimal nanoparticle

dispersion and strong filler–matrix interaction [46-50]. At 5 wt.% TiO_2, the strength decreases slightly to 27.2 MPa, likely due to particle agglomeration that reduces reinforcement efficiency. Overall, the results confirm that 3 wt.% TiO_2 provides the best compressive performance, consistent with densification and structural optimization observed in other characterization results [51,52].

Table 5 Compressive strength values for PVA-CNT-TiO_2 nanocomposites.

Sample	Compressive Strength σ_c (MPa)
Pure PVA	18.2
CNT–0.4%	26.1
PVA–CNT–0.4%–1 wt.% TiO_2	26.1
PVA–CNT–0.4%–3 wt.% TiO_2	29.8
PVA–CNT–0.4%–5 wt.% TiO_2	27.2

4. CONCLUSIONS

In this study, PVA–CNT–TiO_2 hybrid nanocomposites were successfully synthesized using the solution casting method, and the effects of TiO_2 loading (1, 3, and 5 wt.%) on structural, thermal, and mechanical properties were comprehensively evaluated. XRD analysis confirmed the coexistence of semi-crystalline PVA, the CNT (002) peak at 25–26°, and characteristic anatase TiO_2 reflections at 25.3°, 37.8°, 48.0°, 53.9°, and 55.1°, with peak intensities increasing as TiO_2 content rose. FTIR spectra showed systematic modifications in O–H and C=O vibrations and the emergence of Ti–O–C features, confirming strong filler–matrix interactions. TEM images revealed the transition from larger rod-like grains at 1 wt.% TiO_2 to more clustered particles at 3 wt.% and much finer grains at 5 wt.%, supported by grain-size distributions centered at ~80 nm, ~86 nm, and ~53 nm, respectively. Physical property measurements demonstrated that density increased from 1.22 to 1.34 g cm^{-3} up to 3 wt.% TiO_2 before slightly decreasing to 1.30 g cm^{-3} at 5 wt.%, while porosity reached a minimum of 14.2% at 3 wt.% TiO_2. Thermal conductivity improved from 0.36 W m^{-1} K^{-1} for pure PVA to 0.63 W m^{-1} K^{-1} for CNT–PVA and peaked at 0.72 $W.m^{-1}.K^{-1}$ for the 3 wt.% TiO_2 composite. Mechanical characterization showed hardness increasing from 46 Shore D for pure PVA to 62 Shore D at 3 wt.% TiO_2, and compressive strength reaching a maximum of 29.8 MPa at the same loading. The 3 wt.% TiO_2 nano-composite consistently exhibited the highest performance across structural, thermal, and mechanical domains, demonstrating optimal dispersion, enhanced filler–matrix bonding, and superior multifunctional properties.

References

[1] M. Abdel-Fattah, J. Polym. Res., 1 (2023) 23. https://doi.org/10.1007/s10965-023-03550-8
[2] M. Rasheed, I. Alshalal, A. A. Rashed, M. A. Sarhan, A. S. Jaber, Indonesian Journal of Electrical Engineering and Computer Science, 33 (2024) 653. https://doi.org/10.11591/ijeecs.v33.i1.pp653-660
[3] F. Boudou, A. Guendouzi, A. Belakredar, M. RASHEED, Notulae Scientia Biologicae, 16 (2024) 13837. https://doi.org/10.55779/nsb16211837
[4] F. Boudou, A. Belakredar, A. Berkane, M. RASHEED, Notulae Scientia Biologicae, 17 (2025) 12183. https://doi.org/10.55779/nsb17212183
[5] K. K. Khudair, F. Boudou, A. Mohammed, A. Sehmi, A. Belakredar, M. S. Ibrahim, Experimental and Theoretical NANOTECHNOLOGY, 10 (2026) 869. https://doi.org/10.56053/10.S.869

Exp. Theo. NANOTECHNOLOGY 10 (2026) 1379-1390
[6] A. R. J. Katae, H. H. Hussein, A. S. Jaber, M. A. Sarhan, M. RASHEED, Experimental and Theoretical NANOTECHNOLOGY, 10 (2026) 795. https://doi.org/10.56053/10.2.795
[7] A. R. J. Katae, H. H. Hussein, A. S. Jaber, M. A. Sarhan, M. RASHEED, Experimental and Theoretical NANOTECHNOLOGY, 10 (2026) 725. https://doi.org/10.56053/10.2.725
[8] I. M. Mohammed, M. Rasheed, AIP Conference Proceedings, 3321 (2025) 020026. https://doi.org/10.1063/5.0289719
[9] M. Enneffati, M. Rasheed, B. Louati, K. Guidara, R. Barillé, Optical and Quantum Electronics, 51 (2019) 1. https://doi.org/10.1007/s11082-019-2015-5
[10] M. S. Ibrahim, T. T. Issa, B. Yaqoob, E. N. Fayyadh, A. Rashid, R. S. Mahmood, Experimental and Theoretical NANOTECHNOLOGY, 10 (2026) 887. https://doi.org/10.56053/10.S.887
[11] A. A. Al-Muntaser, R. A. Pashameah, E. Alzahrani, S. A. AlSubhi, S. T. Hameed, M. A. Morsi, Journal of Polymers and the Environment, 31 (2022) 2534. https://doi.org/10.1007/s10924-022-02748-z
[12] H. K. Aity, M. Rasheed, E. Dhahri, A. A. Hateef, T. Saidani, Journal of Materials Science, 61 (2026) 6226. https://doi.org/10.1007/s10853-026-12241-w
[13] A. Khaleefah, M. RASHEED, Experimental and Theoretical NANOTECHNOLOGY, 10 (2026) 289. https://doi.org/10.56053/10.s.289
[14] A. I. A. Ali, M. RASHEED, Experimental and Theoretical NANOTECHNOLOGY, 10 (2026) 277. https://doi.org/10.56053/10.s.277
[15] A. I. A. Ali, M. RASHEED, Experimental and Theoretical NANOTECHNOLOGY, 10 (2026) 239. https://doi.org/10.56053/10.s.239
[16] M. Rasheed, M. N. Mohammedali, F. A. Sadiq, M. A. Sarhan, T. Saidani, Journal of Optics, 54 (2024) 1. https://doi.org/10.1007/s12596-024-01928-5
[17] H. M. I. Al-Zuhairi, I. Alshalal, H. H. Abbood, M. Al Nuaimi, Experimental and Theoretical NANOTECHNOLOGY, 10 (2026) 855. https://doi.org/10.56053/10.S.855
[18] H. M. I. Al-Zuhairi, I. Alshalal, H. H. Abbood, M. Al Nuaimi, Experimental and Theoretical NANOTECHNOLOGY, 10 (2026) 1093. https://doi.org/10.56053/10.S.1093
[19] S. S. Batros, M. Rasheed, H. K. Aity, A. A. Hatef, T. Saidani, Materials Chemistry and Physics, 355 (2026) 132243. https://doi.org/10.1016/j.matchemphys.2026.132243
[20] Z. S. Ahmed, M. RASHEED, H. S. Ahmed, Experimental and Theoretical NANOTECHNOLOGY, 10 (2026) 329. https://doi.org/10.56053/10.s.329
[21] Z. S. Ahmed, M. RASHEED, H. S. Ahmed, Experimental and Theoretical NANOTECHNOLOGY, 10 (2026) 343. https://doi.org/10.56053/10.s.343
[22] A. Zubaidi, L. M. Asaad, I. Alshalal, M. Rasheed, Journal of the Mechanical Behavior of Materials, 32 (2023) 1. https://doi.org/10.1515/jmbm-2022-0302
[23] T. Saidani, M. Rasheed, I. Alshalal, A. A. Rashed, M. A. Sarhan, R. Barillé, Research on Engineering Structures and Materials, 9 (2023) 1. https://doi.org/10.17515/resm2023.21ma0922rs
[24] M. Rasheed, et al., Journal of Advanced Biotechnology and Experimental Therapeutics, 6 (2023) 495. https://doi.org/10.5455/jabet.2023.d144
[25] E. Kadri, et al., Journal of Alloys and Compounds, 705 (2017) 708. https://doi.org/10.1016/j.jallcom.2017.02.117
[26] M. Rasheed, R. Barillé, Journal of Alloys and Compounds, 728 (2017) 1186. https://doi.org/10.1016/j.jallcom.2017.09.084
[27] R. S. Mahmood, et al., Journal of the Mechanical Behavior of Materials, 34 (2025) 1. https://doi.org/10.1515/jmbm-2025-0040
[28] M. Enneffati, B. Louati, K. Guidara, M. Rasheed, R. Barillé, Journal of Materials Science: Materials in Electronics, 29 (2018) 171. https://doi.org/10.1007/s10854-017-7901-7

Exp. Theo. NANOTECHNOLOGY 10 (2026) 1379-1390
[29] F. Dkhilalli, S. Megdiche, K. Guidara, M. Rasheed, R. Barillé, M. Megdiche, Ionics, 24 (2018) 169. https://doi.org/10.1007/s11581-017-2193-8
[30] A. Keziz, M. Rasheed, M. Heraiz, F. Sahnoune, A. Latif, Ceramics International, 49 (2023) 37423. https://doi.org/10.1016/j.ceramint.2023.09.068
[31] F. Boudou, A. E. Sabar, M. I. Majeed, A. M. Ibraham, R. Jamal, A. Rashid, A. Belakredar, M. Bendahmane-Salmi, M. RASHEED, R. RASHEED, T. Saidani, H. D. Al-Bahadli, Experimental and Theoretical NANOTECHNOLOGY, 10 (2026) 821. https://doi.org/10.56053/10.S.821
[32] D. Kherifi, A. Keziz, M. Rasheed, A. Oueslati, Ceramics International, 50 (2024) 1. https://doi.org/10.1016/j.ceramint.2024.05.317
[33] A. J. Hussein, M. N. Al-Darraji, M. Rasheed, M. A. Sarhan, IOP Conference Series: Earth and Environmental Science, 1262 (2023) 022005. https://doi.org/10.1088/1755-1315/1262/2/022005
[34] H. K. Aity, E. Dhahri, M. Rasheed, Ceramics International, 50 (2024) 54666. https://doi.org/10.1016/j.ceramint.2024.10.324
[35] W. Saidi, N. Hfaidh, M. Rasheed, M. Girtan, A. Megriche, M. El Maaoui, RSC Advances, 6 (2016) 68819. https://doi.org/10.1039/c6ra15060h
[36] A. J. Hussein, M. N. Al-Darraji, M. Rasheed, IOP Conference Series: Earth and Environmental Science, 1262 (2023) 022007. https://doi.org/10.1088/1755-1315/1262/2/022007
[37] T. Saidani, S. Mokhtari, M. Rasheed, H. Lahmar, M. Trari, Journal of the Indian Chemical Society, 103 (2026) 102499. https://doi.org/10.1016/j.jics.2026.102499
[38] A. Raghdi, M. Heraiz, M. Rasheed, A. Keziz, Journal of the Indian Chemical Society, 101 (2024) 101413. https://doi.org/10.1016/j.jics.2024.101413
[39] T. Rashid, M. M. Mokji, M. Rasheed, Journal of the Mechanical Behavior of Materials, 34 (2025) 1. https://doi.org/10.1515/jmbm-2025-0074
[40] A. A. Hateef, E. Dhahri, M. Rasheed, H. Kadhim, Z. Abbas, N. Hassan, Physics and Chemistry of Solid State, 25 (2024) 801. https://doi.org/10.15330/pcss.25.4.801-810
[41] T. Rashid, M. M. Mokji, M. Rasheed, Journal of Optics, 53 (2024) 1. https://doi.org/10.1007/s12596-024-02080-w
[42] E. Arif, R. Jamal, M. RASHEED, Experimental and Theoretical NANOTECHNOLOGY, 10 (2026) 453. https://doi.org/10.56053/10.2.453
[43] G. E. Alkinani, A. R. J. Katae, M. RASHEED, Experimental and Theoretical NANOTECHNOLOGY, 10 (2026) 1027. https://doi.org/10.56053/10.S.1027
[44] T. Saidani, M. Zaabat, M. S. Aida, R. Barillé, M. Rasheed, Y. Almohamed, Journal of Materials Science: Materials in Electronics, 28 (2017) 9252. https://doi.org/10.1007/s10854-017-6660-9
[45] M. Rasheed, A. Khaleefah, Materials Chemistry and Physics, 355 (2026) 132112. https://doi.org/10.1016/j.matchemphys.2026.132112
[46] F. Boudou, et al., Notulae Scientia Biologicae, 17 (2025) 12593. https://doi.org/10.55779/nsb17312593
[47] M. Rasheed, S. Shihab, O. Alabdali, A. Rashid, T. Rashid, Journal of Physics: Conference Series, 1999 (2021) 012077. https://doi.org/10.1088/1742-6596/1999/1/012077
[48] A. Aukštuolis, et al., Proceedings of the Romanian Academy Series A: Mathematics, Physics, Technical Sciences, Information Science, 18 (2017) 34. https://hal.archives-ouvertes.fr/hal-02443179
[49] E. Kadri, M. Krichen, R. Mohammed, A. Zouari, K. Khirouni, Optical and Quantum Electronics, 48 (2016) 1. https://doi.org/10.1007/s11082-016-0812-7
[50] M. Rasheed, O. Y. Mohammed, S. Shihab, A. Al-Adili, Journal of Physics: Conference Series, 1795 (2021) 012042. https://doi.org/10.1088/1742-6596/1795/1/012042
[51] A. A. Abdulrahman, M. Rasheed, S. Shihab, Journal of Physics: Conference Series, 1879 (2021) 022118. https://doi.org/10.1088/1742-6596/1879/2/022118

[52] A. Jaber, M. Ismael, T. Rashid, M. A. Sarhan, M. Rasheed, I. M. Sala, Eureka: Physics and Engineering, 4 (2023) 29. https://doi.org/10.21303/2461-4262.2023.002770